

Interpretable Failure Analysis in Multi-Agent Reinforcement Learning Systems

Risal Shahriar Shefin*
Wake Forest University
Winston-Salem, NC, USA
shefrs24@wfu.edu

Thai Le
Indiana University
Bloomington, IN, USA
tle@iu.edu

Debashis Gupta*
Wake Forest University
Winston-Salem, NC, USA
guptd23@wfu.edu

Sarra Alqahtani
Wake Forest University
Winston-Salem, NC, USA
sarra-alqahtani@wfu.edu

ABSTRACT

Multi-Agent Reinforcement Learning (MARL) is increasingly deployed in safety-critical domains, yet methods for interpretable failure detection and attribution remain underdeveloped. We introduce a two-stage gradient-based framework that provides interpretable diagnostics for three critical failure analysis tasks: (1) detecting the true initial failure source (PATIENT-0); (2) validating why non-attacked agents may be flagged first due to domino effects; and (3) tracing how failures propagate through learned coordination pathways. Stage 1 performs interpretable per-agent failure detection via Taylor-remainder analysis of policy-gradient costs, declaring an initial PATIENT-0 candidate at the first threshold crossing. Stage 2 provides validation through geometric analysis of critic derivatives-first-order sensitivity and directional second-order curvature aggregated over causal windows to construct interpretable contagion graphs. This approach explains “downstream-first” detection anomalies by revealing pathways that amplify upstream deviations. Evaluated across 500 episodes in Simple Spread (3 and 5 agents) and 100 episodes in StarCraft II using MADDPG and HATRPO, our method achieves 88.2–99.4% PATIENT-0 detection accuracy while providing interpretable geometric evidence for detection decisions. By moving beyond black-box detection to interpretable gradient-level forensics, this framework offers practical tools for diagnosing cascading failures in safety-critical MARL systems.

KEYWORDS

Multi-Agent Reinforcement Learning (MARL); Explainability; Patient Zero Detection

ACM Reference Format:

Risal Shahriar Shefin, Debashis Gupta, Thai Le, and Sarra Alqahtani. 2026. Interpretable Failure Analysis in Multi-Agent Reinforcement Learning Systems. In *Proc. of the 25th International Conference on Autonomous Agents and Multiagent Systems (AAMAS 2026)*, Paphos, Cyprus, May 25 – 29, 2026, IFAAMAS, 9 pages. <https://doi.org/10.65109/GWFE6009>

*These authors contributed equally to this research, and their orders are interchangeable.



This work is licensed under a Creative Commons Attribution International 4.0 License.

Proc. of the 25th International Conference on Autonomous Agents and Multiagent Systems (AAMAS 2026), C. Amato, L. Dennis, V. Mascardi, J. Thangarajah (eds.), May 25 – 29, 2026, Paphos, Cyprus. © 2026 International Foundation for Autonomous Agents and Multiagent Systems (www.ifaamas.org). <https://doi.org/10.65109/GWFE6009>

1 INTRODUCTION

Multi-Agent Reinforcement Learning (MARL) has emerged as a pivotal framework for coordinating autonomous systems across safety-critical domains including robotic fleets, transportation systems, communication networks, and power grids [4, 19–22, 25]. In these settings, where multiple learned policies interact, a single local deviation can ripple through the entire team causing other agents to fail [16].

However, understanding *how* failures propagate in MARL systems presents unique challenges. In tightly coupled multi-agent systems, the first agent to show detectable instability may not be the true failure source; much like a domino effect where the first domino pushed (true source) might fall slowly, while a downstream domino (affected agent) falls dramatically due to amplification. This phenomenon creates fundamental diagnostic challenges: an agent might be flagged as failing first simply because it’s more sensitive to perturbations, while the true root cause remains hidden upstream. In such circumstances, practitioners need explanations that reveal three critical aspects: *who* truly deviated first, *why* certain agents were affected before others, and *how* the deviation propagated through the system. We posit that answers to these questions are paramount and that *safety in MARL is inseparable from explainability and transparency*: only by making agents’ behavior and their interdependencies legible can practitioners debug, test, and ultimately trust these systems.

Despite these needs, explainable MARL (xMARL) remains under-explored. Shapley-value attribution [6, 13] has been used to quantify each agent’s contribution to team reward in cooperative scenarios. Although such attribution offers insights into credit assignment, it does *not* reveal inter-agent dynamics or cascading failures. Complementary work [5] provides policy-level contrastive explanations by checking user-specified temporal task queries against abstracted policies via probabilistic model checking. While valuable, these approaches are not designed to analyze failure dynamics in team settings, such as how failures unfold, which agent was the inciting point of failure, and why.

In contrast, single-agent Explainable RL (XRL) has recently shifted toward safety debugging and testing, using explanations to surface vulnerabilities and guide falsification (e.g., [12, 23]). For instance, xSRL [23] combines local post-hoc explanations with global abstract policy graphs to identify and patch safety violations. AEGIS-RL [12] builds on xSRL by developing a verification approach that integrates

formal model checking with risk- and uncertainty-guided falsification. However, repurposing these single-agent methods for MARL is not straightforward due to the heightened complexity of multi-agent systems. The explainability challenge in MARL surpasses that of single-agent RL, primarily due to the inherent coupling and dependencies among agents. While single-agent explanations can focus on an individual policy, MARL requires untangling a web of interdependencies, compounded by emergent collective behaviors and environmental non-stationarity. These dynamic feedback loops obscure cause-effect relationships, making it difficult to distinguish between agent-level and system-level failures.

Moreover, conventional failure analysis in MARL often tracks global metrics such as team reward or derived statistics over time [2, 26]. Such global performance metrics can obscure policy instability in individual agents [1, 9] as we show in our experiments. Moreover, they neither identify the first agent to enter a non-robust state nor reveal how deviations propagate, all of which are needed to pinpoint weak points and pathways for proactive mitigation.

Therefore, this paper formalizes the interpretable failure analysis problem in MARL around three core questions; **Q1**. Who is the true PATIENT-0: the first agent to enter a non-robust state?, **Q2**. Why might a non-attacked agent be flagged first? How do we distinguish true sources from amplified downstream effects?, and **Q3**. How does instability propagate across agents over time through the system’s learned coordination pathways? We propose to address these questions through a two-stage, gradient-based forensic method. Stage 1 performs per-agent local detection by probing the Taylor-error of a policy-gradient cost; the earliest threshold crossing declares an initial PATIENT-0 candidate (Q1). Stage 2 validates or corrects this candidate by tracing accelerating upstream influence using critic derivatives-first- and second-order action sensitivities aggregated over causal windows (Q2). This approach naturally yields constructions of directed contagion graphs that summarize propagation pathways, influence strength, and timing (Q3).

Contributions. We make four main contributions:

- (1) **Two-stage PATIENT-0 detection.** A gradient-based method that combines local policy instability detection with upstream traceback validation.
- (2) **Geometric explanation of detection anomalies.** Directional second-order analysis distinguishes accelerating vs. damping influence, explaining why downstream agents might be flagged before true sources.
- (3) **Interpretable contagion graphs.** Directed graphs that quantitatively capture influence strength, amplification frequency, and propagation timing.
- (4) **Comprehensive evaluation.** Across two environments and two algorithms, we report PATIENT-0 identification accuracy of 88.2% – 99.4% with intervention studies validating that perturbing high-influence, accelerating states induces significantly longer instability.

By moving beyond team reward to gradient-level influence analysis, our approach provides actionable insight into systemic vulnerabilities, revealing not just which agent failed first, but *why* and *through which pathways* failures spread, enabling more reliable MARL testing and deployment in safety-critical domains.

2 RELATED WORK

Explainability in MARL (xMARL). Research in explainable MARL is limited and primarily splits into (i) credit assignment [6, 13] and (ii) specification- or query-driven explanations [5]. Shapley-based methods [6, 13] quantify each agent’s contribution to the team reward, offering insights into fairness and cooperation but not into failure dynamics or inter-agent cascades. Recent work continues to advance credit assignment, such as Multi-level Advantage Credit Assignment (MACA) [27], which performs counterfactual reasoning across different levels of agent coordination but remains focused on optimizing training rather than diagnosing post-hoc failures. Complementarily, policy-level contrastive explanations [5] verify temporal task queries (e.g., encoded in PCTL*) via probabilistic model checking on an abstracted policy. While both lines illuminate aspects of MARL behavior, neither targets post-hoc failure analysis under compromised agents: they do not identify the entry point of a failure nor reconstruct how influence propagates across agents over time. Our method addresses this gap by detecting the first non-robust agent and mapping directed, time-resolved propagation paths using centralized-critic sensitivities.

Single-agent XRL and Policy Summaries. A rich body of XRL provides explanations for a single agent, including policy summarization via abstract policy graphs [3, 18], contrastive explanation methods [24], and frameworks that integrate local and global summaries [12, 23]. Safety-focused XRL (e.g., xSRL [23]) ties explanations to debugging and patching unsafe behavior but remains single-agent in scope. Directly porting these methods to MARL misses the core challenge: the coupling and non-stationarity among agents obscure cause-effect relations across the team. Our work departs by explicitly modeling cross-agent influence during failure episodes and delivering a cascade map that explains how a local deviation spreads at run time.

Attacks and Robustness. The vulnerability of cooperative MARL to adversarial pressure is well-studied, including attacks that degrade team performance [7, 14–16]. These works establish vulnerabilities and propose defenses, but generally focus on performance degradation or anomalous behavior detection without explaining the failure’s origin and propagation pathway. Our contribution is orthogonal and complementary: a post-hoc explainer that identifies PATIENT-0 and attributes influence across agents.

3 APPROACH

We propose a two-stage, interpretable gradient-based method for MARL failure forensics. The key insight is that a failure typically begins with one agent and then propagates via learned coordination. Stage 1 performs per-agent local detection by probing policy-gradient Taylor error and declares PATIENT-0 as the first threshold crossing. Stage 2 validates or corrects it by tracing accelerating upstream influence using critic derivatives-first-order sensitivity and directional curvature-aggregated over a short causal window. These scores yield a directed contagion graph that summarizes who influenced whom, the strength and frequency of amplification, and how quickly deviations spread. We assume a single failure entry per episode, with subsequent failures arising from cascades through cooperative coupling.¹

¹Relaxing the single-entry assumption is left to future work.

3.1 Two-Stage PATIENT-0 Detection and Validation

In tightly coupled multi-agent systems, the first agent to show detectable instability may not be the true failure source. Consider a domino effect: the first domino pushed (true source) might fall slowly, while a downstream domino (affected agent) falls dramatically due to amplification. Stage 1 identifies which domino fell first; Stage 2 traces back to find who pushed it.

Stage 1: Local Policy Instability via Taylor Remainder. We monitor each agent’s policy stability by measuring sensitivity to small observation perturbations. The key intuition: when policies enter fragile states, small changes in observations cause disproportionately large changes in policy update directions.

For agent i with policy $\pi_i(a | o_i)$, we define the action commitment cost:

$$J_i(o_i, \tau_i) = - \sum_a \tau_i(a) \log \pi_i(a | o_i), \quad (1)$$

$$\tau_i(a) \equiv \pi_i^*(a | o_i^t) = \mathbb{1}_{a=\arg \max_{a'} \pi(a' | o_i^t)}.$$

By fixing τ_i at the current greedy action, we transform policy evaluation into a deterministic function of observations. Gradients and Hessians are taken w.r.t. observations with τ_i held fixed:

$$\nabla_{o_i} J_i(o_i^t, \tau_i), \quad \nabla_{o_i}^2 J_i(o_i^t, \tau_i).$$

For a small perturbation η_i , Taylor’s theorem gives:

$$J_i(o_i^t + \eta_i, \tau_i) = J_i(o_i^t, \tau_i) + \nabla_{o_i} J_i(o_i^t, \tau_i)^\top \eta_i + \frac{1}{2} \eta_i^\top \nabla_{o_i}^2 J_i(o_i^t, \tau_i) \eta_i,$$

for some $\tilde{o}_i \in [o_i^t, o_i^t + \eta_i]$. We define the Taylor remainder statistic:

$$\mathcal{L}_i^t(\eta_i) \triangleq J_i(o_i^t + \eta_i, \tau_i) - \left(J_i(o_i^t, \tau_i) + \nabla_{o_i} J_i(o_i^t, \tau_i)^\top \eta_i \right), \quad (2)$$

so that for small η_i , $\mathcal{L}_i^t(\eta_i) \approx \frac{1}{2} \eta_i^\top \nabla_{o_i}^2 J_i(o_i^t, \tau_i) \eta_i$. This provides a curvature probe in observation space without forming the full Hessian, similar to the Second-Order Identification of Non-Robust Directions test from single-agent RL [10]. Large deviations indicate the policy is in a non-robust, high-curvature region where small observation changes could cause large policy shifts.

This local per-agent policy curvature test is effective in MARL because during decentralized execution, each agent i executes its policy based solely on local observations o_i , which implicitly encode teammates’ behavior through environment dynamics. A deviation by any agent perturbs others’ observation manifolds, altering the local geometry of $J_i(o_i)$. Thus, monitoring the directional curvature of J_i with respect to o_i serves as a policy-agnostic, per-agent detector of entry into non-robust state without requiring explicit inter-agent communication or access to peers’ policies.

Then, from fault-free rollouts, we establish baseline stability profiles for each agent. During failure episodes, we flag agents when their Taylor-error significantly exceeds their normal operating range. The earliest-detected agent becomes our initial PATIENT-0 candidate:

$$\hat{p}_{S1} = \arg \min_i T_i, \quad \hat{T}_{\text{attack}} = T_{\hat{p}_{S1}}. \quad (3)$$

, where T_i is the time when agent i is flagged.

Stage 2: Cascade Source Identification via Directional Critic Curvature. Stage 1 can be misled by downstream-first cascades, where a non-source agent crosses the instability threshold before

the true origin. This happens when small upstream deviations are amplified at sensitive teammates, when observation coupling causes agents to indirectly “see” each other through the environment dynamics, or when the system passes through critical coordination states that magnify otherwise minor perturbations. To disambiguate these cases, we perform a directional second-order analysis on the critic: first-order sensitivities identify who most strongly affects whom, while the directional curvature of the critic isolates amplifying (vs. damping) states, allowing us to traceback the highest-leverage upstream source and validate or correct the Stage 1 PATIENT-0.

In MARL algorithms with action-value critic (e.g., MADDPG [17]), we leverage the trained per-agent critic $Q_i(s, a_1, \dots, a_n)$ that conditions on the global state (or joint observations) and the joint action; this object encodes inter-agent dependencies learned during training. In algorithms that only learn a state-value function (e.g., HATRPO [11]), we fit a light post-hoc probe critic $\tilde{Q}_i(s, a_1, \dots, a_n)$ on frozen rollouts for attribution only (not for control), by regressing to TD or Monte-Carlo targets.² This yields well-defined partials $\partial Q_i / \partial a_j$ and $\partial^2 Q_i / \partial a_j^2$ that quantify how agent j ’s action locally perturbs agent i ’s value and, by extension, its policy’s stability signals. We define the critic cost function as $L_{Q_i} = -Q_i$, thereby treating higher values as worse and lower values as better, which preserves the standard characteristics of a cost function.

For an ordered pair ($j \rightarrow i$) at (s_t, a_t) , let

$$\mathbf{g}_{ij}^t = \frac{\partial L_{Q_i}(s_t, a_t)}{\partial a_j}, \quad \mathbf{H}_{ij}^t = \frac{\partial^2 L_{Q_i}(s_t, a_t)}{\partial a_j^2}.$$

We use the first-order influence magnitude $G_{ij}^t = \|\mathbf{g}_{ij}^t\|_2$ and the directional second-order term

$$D_{ij}^t = \mathbf{g}_{ij}^{t\top} \mathbf{H}_{ij}^t \mathbf{g}_{ij}^t, \quad (4)$$

which evaluates curvature along the locally most sensitive direction. Under a second-order Taylor expansion of \mathcal{L}_{Q_i} with respect to a_j ,

$$\Delta \mathcal{L}_{Q_i} \approx \mathbf{g}_{ij}^{t\top} \delta a_j + \frac{1}{2} \delta a_j^\top \mathbf{H}_{ij}^t \delta a_j.$$

When G_{ij}^t is large and $D_{ij}^t > 0$, small deviations in a_j are *amplified* at i (accelerating influence); when $D_{ij}^t < 0$, they are *damped* (saturating influence). This explains how a teammate i can exhibit an earlier curvature spike than the true source agent (true PATIENT-0 j).

To validate \hat{p}_{S1} (Eq.3) in Stage-1, we trace potential harmful upstream over a short window ending at the detection time, aggregating only the accelerating portions:

$$I_{j \rightarrow i} = \sum_{t=t_0}^{t_1} \omega(t_1-t) \mathbb{1}\{D_{ij}^t > 0\} |\mathcal{L}_j^t(\eta_j) - E\{\mathcal{L}_j^t\}|, \quad (5)$$

where $[t_0, t_1]$ is a causal window (e.g., $t_1 = T_i$ and $t_0 = \max\{0, T_j\}$), $\omega(\cdot)$ is a recency weight, $I_{j \rightarrow i}$ is cumulative (accelerating) deviation impact, and $E\{\mathcal{L}_j^t\}$ denotes the expected baseline of \mathcal{L}_j^t obtained from the previously computed stability profiles. We then iteratively move from the detected agent to its strongest accelerating upstream source until no stronger source is found (or a cycle would form).

²Either critic is required only to be differentiable with respect to each action argument so that we can take first- and second-order derivatives. For discrete actions we use a standard continuous relaxation (e.g., softmax with temperature or Gumbel-Softmax during probing); for continuous actions we directly backpropagate.

Algorithm 1 Traceback Validation of PATIENT-0 with Directional Second Order

Require: Stage-1 \hat{p}_{S1} at time t^* ; window K ; decay ω

- 1: $\text{curr} \leftarrow \hat{p}_{S1}$, $\text{chain} \leftarrow [\text{curr}]$, $\mathcal{W} \leftarrow \{t^*-K, \dots, t^*\}$
- 2: **while** true **do**
- 3: **for all** $j \neq \text{curr}$ **do**
- 4: $I_{j \rightarrow \text{curr}} \leftarrow \sum_{t \in \mathcal{W}} \omega(t^*-t) \mathbf{1}\{D_{\text{curr},j}^t > 0\} |\mathcal{L}_j^t(\eta_j) - E\{\mathcal{L}_j^t\}|$
- 5: **end for**
- 6: $j^* \leftarrow \arg \max_j I_{j \rightarrow \text{curr}}$
- 7: **if** $I_{j^* \rightarrow \text{curr}}$ is negligible **or** $j^* \in \text{chain}$ **then**
- 8: **break**
- 9: **end if**
- 10: append j^* to chain; $\text{curr} \leftarrow j^*$
- 11: **end while**
- 12: **return** chain (upstream sources ending at \hat{p}_{S1})

The traceback (Algorithm 1) hence validates Stage-1 by (i) revealing whether the Stage-1 flag lies on a high-influence, accelerating edge from an upstream agent, and (ii) identifying that upstream agent.

Remarks. Stage-1’s Taylor-error \mathcal{L}_i^t (Eq. (2)) probes directional curvature of the policy-gradient norm $J_i(o_i)$ (Eq. (1)). Stage-2 traces cross-agent influence using critic derivatives $\mathbf{g}_{ij}^t = \partial Q_i / \partial a_j$ and $\mathbf{H}_{ij}^t = \partial^2 Q_i / \partial a_j^2$ as practical proxies for environmental coupling (under a mild critic–influence alignment on the analysis window). The directional curvature $D_{ij}^t = \mathbf{g}_{ij}^{t\top} \mathbf{H}_{ij}^t \mathbf{g}_{ij}^t$ (Eq. (4)) decomposes as $D_{ij}^t = \|\mathbf{g}_{ij}^t\|_2^2 \kappa_{ij}^t$ with κ_{ij}^t the Rayleigh quotient. When $D_{ij}^t > 0$ (accelerating states) and $G_{ij}^t = \|\mathbf{g}_{ij}^t\|_2$ is large, small perturbations δa_j can disproportionately amplify downstream agents’ Taylor-errors, explaining “downstream-first” flags. Accordingly, our traceback aggregates only accelerating edges ($D_{ij}^t > 0$) to validate or correct the Stage-1 candidate \hat{p}_{S1} (Eq. (3)). Appendix A provides a short lemma and proposition formalizing these links.

3.2 Cross-Agent Action Influence for Cascade Attribution

The influence magnitude G_{ij}^t , and directional derivative D_{ij}^t naturally yield a weighted, directed graph where edges $j \rightarrow i$ represent influence pathways. Edge weights combine G_{ij} (first-order sensitivity) and the frequency of accelerating states ($D_{ij}^t > 0$). By thresholding on cumulative influence $I_{j \rightarrow i}$, we extract the salient contagion subgraph that explains failure propagation.

Let t_i denote agent i ’s detection time (first Taylor-error exceedance). For each subsequently failing agent k and candidate predecessor j with $t_j \leq t_k$, we define the attribution window:

$$\mathcal{W}_{j \rightarrow k} = \{t_j, t_{j+1}, \dots, t_k\}.$$

This focuses analysis on the interval between upstream detection and downstream failure.

For each pair ($j \rightarrow k$), we compute three interpretable summaries over $\mathcal{W}_{j \rightarrow k}$:

$$IS_{j \rightarrow k} = \frac{1}{|\mathcal{W}_{j \rightarrow k}|} \sum_{t \in \mathcal{W}_{j \rightarrow k}} G_{kj}^t, \quad (6)$$

$$CR_{j \rightarrow k} = \frac{100}{|\mathcal{W}_{j \rightarrow k}|} \sum_{t \in \mathcal{W}_{j \rightarrow k}} \mathbf{1}\{G_{kj}^t \geq \theta_G \wedge \tilde{D}_{kj}^t > 0\}, \quad (7)$$

$$t_{j \rightarrow k} = [t_k, t_j]. \quad (8)$$

Here $\bar{I}S_{j \rightarrow k}$ is the influence score (magnitude), $CR_{j \rightarrow k}$ is the percentage of critical leverage steps (high influence with positive curvature), and $t_{j \rightarrow k}$ is the detection time period. Threshold θ_G is set to a robust scale (e.g., episode median).

We rank candidate predecessors using a score that combines our existing signals:

$$S_{j \rightarrow k} = \sum_{t \in \mathcal{W}_{j \rightarrow k}} \omega(t_k - t) \max(\tilde{D}_{kj}^t, 0) G_{kj}^t, \quad \omega(\cdot) \in (0, 1] \text{ monotone.}$$

We retain edge $j \rightarrow k$ if $S_{j \rightarrow k}$ exceeds fraction τ of k ’s top score (e.g., $\tau = 0.5$ for salient secondary parents).

We then construct a directed contagion graph over agents in detection order. Each node shows agent ID and policy instability occupancy IO_i ; the number of timesteps the policy remained unstable due to incoming influences, measured from first to last Taylor-error exceedance. Each retained edge $j \rightarrow k$ reports $IS_{j \rightarrow k}$; $CR_{j \rightarrow k}\%$; $t_{j \rightarrow k}$ steps.

This contagion graph integrates all analytical components in a single view: direction (who influenced whom, via edge orientation), strength (total influence magnitude, IS), geometry (amplification frequency, CR), timing (the propagation period, t), and instability occupancy (IO , the timesteps during which an agent’s policy was unstable under inbound influence). This integrated summary reveals both the severity of impact on individual agents and the mechanistic routes through which failures spread and amplify throughout the system.

4 EXPERIMENTS

We evaluate our two-stage failure-analysis framework across multiple environments and algorithms to address three questions: **Q1:** How accurately does the method identify the true PATIENT-0? **Q2:** Why are non-attacked agents sometimes flagged first, and can traceback correct them? **Q3:** Do the influence scores provide actionable, episode-level insight into how failures propagate?. All the codes relevant to the experiments are available online³.

4.1 Setup

Environments and algorithms. We use Simple Spread (cooperative navigation) with $n \in \{3, 5\}$ agents and SMAC (Starcraft II). In Simple Spread, n agents must navigate to L landmarks through coordinated movement. Agents observe relative positions of other agents and landmarks, and receive shared rewards to minimize distance to landmarks. SMAC is a decentralized micromanagement benchmark where 3 Marine agents must defeat 3 Zealot opponents through coordinated focus fire and positioning. Each agent receives partial

³<https://github.com/risal-shefin/marl-failure-analysis>

observations and controls one Marine unit, requiring emergent coordination strategies to overcome the enemy’s statistical advantages. We tested two MARL algorithms; MADDPG [17] and HATRPO [11].

Failure Simulation/ Intervention Protocol. We simulate failures using the worst-action attack from adversarial MARL [14, 16]. We then created an intervention protocol to test our proposed work. For each ordered pair ($j \rightarrow i$), we intervene at two classes of timesteps computed from the trained critic(s): *Critical* states where G_{ij} is high and $D_{ij} > 0$, and *Robust* states where G_{ij} is low and $D_{ij} \leq 0$. We replace a_j with the same-strength attack action in both conditions and compare outcomes over an identical window W . Per environment this yields 500 base episodes \times ordered pairs $\times 2$ conditions: 6,000 variants for $n=3$ (6 pairs), and 20,000 for $n=5$ (20 pairs). For the SMAC 3s_vs_3z, we experimented with 100 base episodes, yielding 1,200 variants in total.

Validation rationale (paired causal test). If G_{ij} truly captures agent j ’s capacity to affect agent i , then interventions at Critical moments (high G_{ij} with $D_{ij} > 0$) should induce more severe downstream instability than identical interventions at Robust moments (low G_{ij} with $D_{ij} \leq 0$). We employ a paired experimental design where both intervention types are applied to the same agent pair ($j \rightarrow i$) within the same episode.

Evaluation Metrics. To validate (PATIENT-0 identification), we report four accuracy measures: Stage-1 accuracy $\Pr(\hat{p}_{S_1}=p^*)$, Traceback accuracy % (chain ends at p^*), Combined accuracy after Stage-2 correction, and Correction rate (the fraction of downstream-first misidentifications successfully corrected by Stage-2, calculated over all downstream-first cases). We didn’t report PATIENT-0 baselines because prior works address different problems: [15] detects per-timestep anomalies using LSTMs on state-action traces without identifying the initial failure source, while [8] develops decentralized GRU-based normality scoring for anomaly detection but does not identify the first inciting agent.

4.2 Results

Results for PATIENT-0 identification (Table. 1). Stage-1 accuracy shows HATRPO consistently outperforming MADDPG ($\Delta+3.4\%$ to $\Delta+10.8\%$ across settings), confirming our hypothesis that smoother gradient landscapes (HATRPO) yield cleaner Taylor-error signals. MADDPG’s exploration noise creates higher gradient jitter, particularly damaging in larger teams (Simple Spread-5: 88.1% vs. HATRPO’s 98.9%).

Stage-2 correction rates reveal the method’s strength in coordinated settings: SMAC achieves 70.8-76.9% correction by leveraging tight coupling dynamics, while Simple Spread-5 MADDPG struggles (40.1%) with diffuse influence across 5 agents. This pattern precisely matches our theoretical expectation: directional curvature effectively traces amplification pathways but requires sufficiently strong coupling signals. The stark contrast between environments highlights this dependency: Simple Spread’s cooperative navigation creates relatively weak, distributed couplings compared to SMAC’s real-time strategy combat, where targeting decisions, focus fire, and ability coordination create intense, immediate interdependencies that our directional curvature term readily detects.

Combined accuracy demonstrates the two-stage design working as intended: substantial gains where Stage-1 struggles (MADDPG: +4.7-8.2% improvements) while maintaining near-perfect performance where Stage-1 already excels.

Results for Influence Validation (Table. 2). Our instability occupancy (IO) metric consistently outperforms traditional performance measures (drop in reward and Q) by 20+ percentage points in most cases (e.g., Simple Spread-3 MADDPG: 77.7% vs. 51.2%/48.4%). Critically, IO remains decisively above chance even when AUC metrics fail, proving gradient geometry captures vulnerability signals invisible to performance-based approaches.

Algorithmic patterns reveal how underlying RL methods affect our metric’s fidelity: HATRPO maintains strong IO accuracy even in complex settings (Simple Spread-5: 82.4%, SMAC: 59.7%) while MADDPG degrades with task complexity (SMAC: 54.5%). This directly aligns with our method’s dependence on stable critic landscapes and precise action gradients. HATRPO’s trust regions and advantage normalization provide these, while MADDPG’s exploration noise and continuous relaxations of discrete actions introduce noise that corrupts our gradient-based signals.

The MADDPG results reveal a key strength of our two-stage design: even with modest Stage-1 IO accuracy (54.5%), Stage-2 achieves strong correction rates (70.8%). This demonstrates that curvature gating can salvage imperfect detection. While Stage-1 may misidentify exactly which agents are unstable, Stage-2’s directional curvature analysis still correctly traces the true amplification pathways through SMAC’s strong, structured couplings. The method proves robust to noisy inputs when the underlying influence topology is clear.

Remarks. (i) When gradient landscapes are smooth (HATRPO), Stage-1 alone is highly accurate; Stage-2 primarily fixes the occasional downstream-first episode (large boost on SMAC). (ii) When gradients are jittery or influence is diffuse (MADDPG in Simple Spread-5), extend the traceback window and allow multi-parent edges to capture split pathways. (iii) For discrete-action tasks like SMAC, using temperature-scheduled Gumbel-Softmax (or an auxiliary probe critic) can improve derivative fidelity and further strengthen IO and correction rates.

4.3 Contagion Graph for Interpretable Failure Analysis.

We present two representative cases that show how the two-stage method detects, explains, and corrects failure dynamics. Throughout, Instability Occupancy (IO) is the “Exceed Rate” in the figures, and edge annotations use Critical Rate (CR) for the frequency of accelerating states ($D_{ij} > 0$) and Influence Score (IS) for cumulative first-order sensitivity (our aggregated G signal). The visuals are organized to align with our pipeline: Stage 1 evidence (Taylor-error and IO timelines) on the left, and Stage 2 evidence (accelerating edges and traceback) on the right.

Case 1 (Simple Spread, $n=3$, MADDPG, edge $2 \rightarrow 0$). We perform two one-shot interventions on the same edge $2 \rightarrow 0$ with the same attack strength and post-intervention horizon K : (i) a *Critical* moment where the local sensitivity is high (large $G_{2 \rightarrow 0}$) and the directional curvature is *accelerating* ($D_{2 \rightarrow 0} > 0$), and (ii) a *Robust* moment where sensitivity is low and/or curvature is non-accelerating

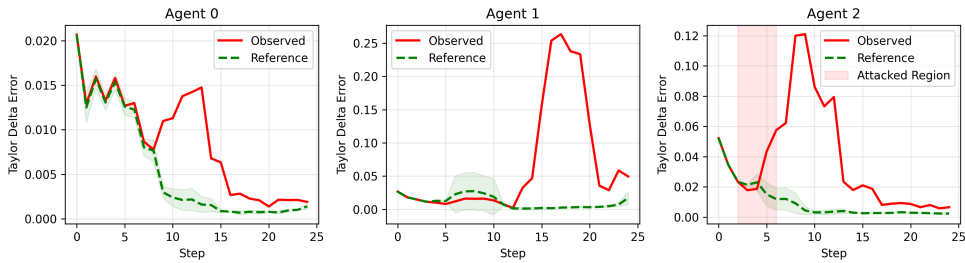
Table 1: PATIENT-0 identification. Columns (left to right): Stage-1 accuracy; Correction Rate (computed only over downstream-first cases); and Combined accuracy after Stage-2 correction.

Setting	Algorithm	Stage-1	Correction Rate	Combined
SimpleSpread-3	MADDPG	95.7%	66.9%	98.6%
	HATRPO	99.1%	66.7%	99.4%
SimpleSpread-5	MADDPG	88.1%	40.1%	92.8%
	HATRPO	98.9%	48.6%	99.2%
SMAC (3s_v_3z)	MADDPG	84.0%	70.8%	88.2%
	HATRPO	94.8%	67.7%	98.3%

Table 2: Influence metric accuracy: Critical state interventions cause significantly longer instability than robust state interventions across the paired scenarios. Our instability occupancy (IO) outperforms traditional performance metrics in revealing vulnerabilities.

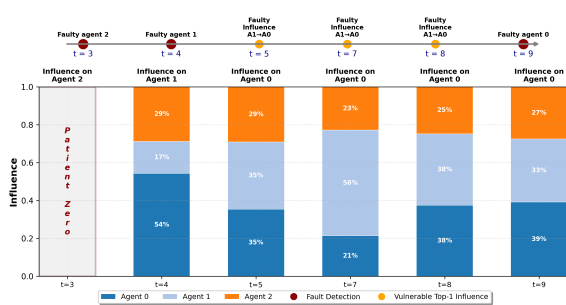
Setting	Algorithm	IO	AUC-Q	AUC-Reward
Simple Spread (3 agents)	MADDPG	77.7%	51.2%	48.4%
	HATRPO	74.0%	59.6%	62.3%
Simple Spread (5 agents)	MADDPG	71.3%	49.9%	51.2%
	HATRPO	82.4%	72.1%	56.6%
SMAC (3s_vs_3z)	MADDPG	54.5%	53.2%	47.7%
	HATRPO	59.7%	45.7%	52.7%

Taylor Expansion Error | Attacked Agent ID: 2

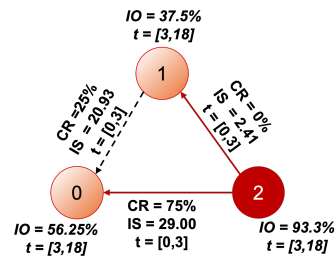


(a) Stage 1: Taylor approximation error in all agents

Fault Detection Timeline with Action Influence Analysis



(b) Stage 1,2: Influence timeline from the detection time of PATIENT-0 to the detection of the last faulty agent

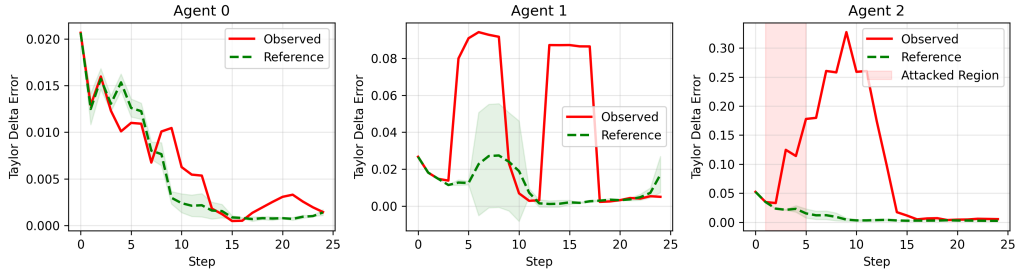


CR = Critical Rate | IS = Influence Score | IO = Instability Occupancy | Patient-0

(c) Stage 1&2: Contagion graph. Nodes with gradient color represent faulty agents

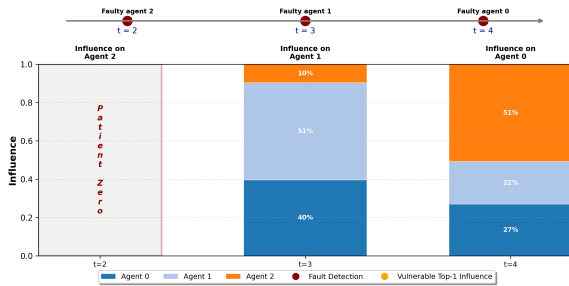
Figure 1: High-influence episode. Top: Stage 1 Taylor-error signals (three agents). Bottom: stacked influence timeline (left) and Stage 2 contagion graph (right), showing dominant accelerating pathways. Notation for time windows: The label $t[\cdot, \cdot]$ on nodes denotes the interval used to evaluate the node's Instability Occupancy (IO): for agent i with detection time T_i , we observe IO from $t[T_i, T_i+15]$. On edges $j \rightarrow i$, the "recent 5" tag denotes the last up-to-5 steps ending at the downstream detection time T_i , i.e., $\{\max(0, T_i-4), \dots, T_i\}$, which are used to compute the edge's Critical Rate (CR) and Influence Score (IS).

Taylor Expansion Error | Attacked Agent ID: 2

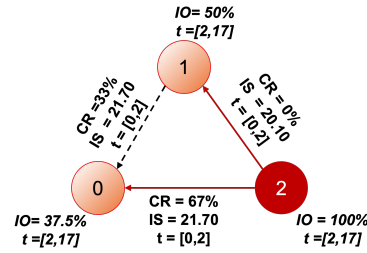


(a) Stage 1: Taylor approximation error in all agents.

Fault Detection Timeline with Action Influence Analysis



(b) Stage 1&2: Influence timeline from the detection of PATIENT-0 to the detection of the last faulty agent.



CR = Critical Rate | IS = Influence Score | IO = Instability Occupancy | Patient-0

(c) Stage 1&2: Contagion graph. Nodes with gradient color represent faulty agents.

Figure 2: Low-influence episode. Top: Stage 1 Taylor-error signals (three agents). Bottom: influence timeline (left) and Stage 2 contagion graph (right), illustrating weaker upstream pathways.

($D_{2 \rightarrow 0} \leq 0$). Figures 1 (high influence) and 2 (low influence) visualize the resulting Stage 1 and Stage 2 signals.

Stage 1: What becomes unstable (and for how long). In the high-influence episode (Fig. 1a), the downstream agent 0 exhibits a clear Taylor-error surge relative to its reference trajectory, and the excursion persists over many steps. This is reflected in a larger instability occupancy (IO) for node 0 over the node window $t[T_0, T_0+15]$ (shown on the node label in the graph). In contrast, in the *low-influence* episode (Fig. 2a), the Taylor-error deviations at agent 0 are notably smaller and shorter, yielding a lower IO over the same evaluation window. Thus, Stage 1 indicates that striking $2 \rightarrow 0$ at a high- G accelerating state produces stronger and more persistent local instability than striking it at a robust moment.

Stage 2: Why it happens (and from where). The stacked influence timelines (Figs. 1b and 2b) align contributions around detection and show how much of agent 0’s update pressure is attributable to each teammate. In the high-influence case, agent 2 contributes a dominant upstream share to agent 0 near T_0 , consistent with a propagating cascade. The contagion graphs (Figs. 1c and 2c) make this causal picture explicit using our directional metrics computed on the *recent-5* edge window $\{\max(0, T_0-4), \dots, T_0\}$ (shown on each edge label): the edge $2 \rightarrow 0$ carries a higher Critical Rate (CR; fraction of steps with $D_{2 \rightarrow 0} > 0$) and a larger Influence Score (IS; masked accumulation of $G_{2 \rightarrow 0}$ over steps with $D > 0$) in the high-influence episode, but both CR and IS are lower in the low-influence episode.

Node labels simultaneously display the IO window $t[T_i, T_i+15]$, tying the downstream instability back to its temporal evaluation range.

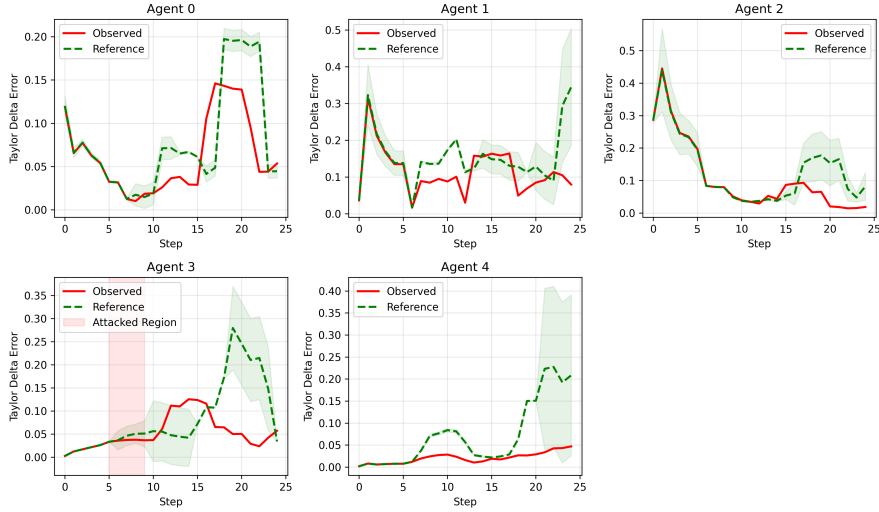
Viewed together, the episodes reveal the mechanism: perturbing the source at a high- G , $D > 0$ state produces stronger, longer downstream instability that Stage 2 traces to an accelerating path (high CR/IS on $2 \rightarrow 0$); perturbing the same edge at a robust (low- G or $D \leq 0$) state yields muted, non-propagating effects (low CR/IS).

Case 2 - Downstream-first flag with traceback correction (Simple Spread, $n=5$, MADDPG). An adversarial perturbation is applied to agent 3 over $t=5-8$. Yet Stage 1 raises the first alarm at agent 1 at $t=7$, creating a downstream-first cascade and a false PATIENT-0.

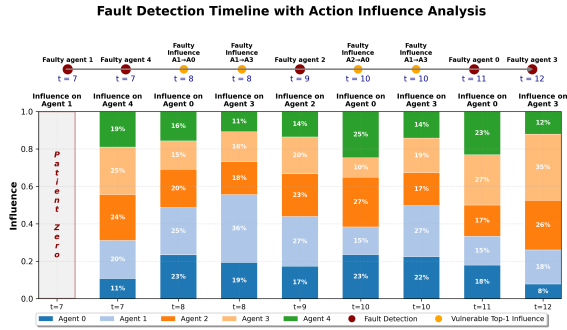
Stage 1: What trips first (and where instability persists). Figure 3a shows agent 1’s Taylor-error crossing the threshold earliest at $t=7$, while agents 0 and 2 exhibit sub-threshold rises and agent 3’s local error remains comparatively muted during the shaded attack window. The instability-occupancy (IO) windows $t[T_i, T_i+15]$ (shown on node labels in Fig. 3c) confirm that agent 1 accrues the earliest and most sustained excursion despite being downstream.

Stage 2: Why agent 1 fires first (and where amplification began). Aligned to T_1 , the stacked influence timeline in Fig. 3b concentrates upstream pressure from $\{3, 2, 0\}$ onto agent 1 immediately before detection. The contagion graph in Fig. 3c gates edges by accelerating directional curvature ($D_{ij} > 0$ over the *recent-5* steps before T_i) and

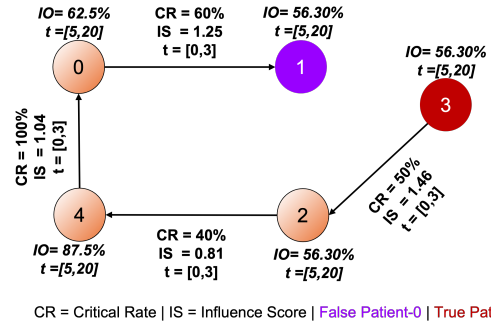
Taylor Expansion Error | Attacked Agent ID: 3



(a) Stage 1: Taylor-approximation error across agents (downstream-first episode).



(b) Influence timeline around detections (stacked upstream shares).



(c) Stage 2: traceback/contagion graph correcting the false PATIENT-0. Nodes with gradient fill are faulty.

Figure 3: False PATIENT-0 (downstream-first) visualization. *Top*: Stage 1 Taylor-error signals lead to an early flag on a downstream agent. *Bottom-left*: Influence timeline shows strong upstream contributions near each detection. *Bottom-right*: Stage 2 traceback via directional critic curvature reveals the true source and the amplifying pathway.

accumulates sensitivity-weighted mass as an Influence Score (IS). This traceback identifies agent 3 as the *true* PATIENT-0 and explains why the receiver (agent 1) crossed the threshold first. Takeaway. Stage 1 alone may nominate a false PATIENT-0 when amplification concentrates on a downstream receiver. Stage 2 corrects this failure mode by (i) gating for accelerating edges ($D > 0$), (ii) weighting by sensitivity (IS), and (iii) aggregating over the *recent-5* causal window recovering the true source (agent 3) and the pathway that carried the pressure to agent 1.

5 DISCUSSION AND CONCLUSION

We introduce, to our knowledge, the first framework for PATIENT-0 detection and influence traceback in MARL. By turning opaque multi-agent failures into critic-geometric evidence and contagion graphs, the method yields actionable forensics for safety-critical deployments: it identifies root causes, explains detection anomalies,

and maps how failures propagate. Our approach is a compact two-stage procedure: Stage 1 flags per-agent onsets from Taylor-error anomalies and summarizes persistence (IO); Stage 2 traces causal routes via directional critic derivatives, emphasizing states with high sensitivity and accelerating curvature. Limitations include a single-source of failure assumption; reliance on differentiable critics and approximate gradient-influence alignment; sensitivity to thresholds and windowing; and added computational cost (gradients and Hessian-vector products). Future work will relax the single-source assumption, reduce overhead with lighter estimators, harden robustness to critic misspecification, and develop online detection at scale on larger, more heterogeneous teams and real deployments.

ACKNOWLEDGMENTS

This material is based upon work supported by the National Science Foundation (NSF) under grant no. 2442581.

REFERENCES

- [1] Sherief Abdallah. 2009. Why Global Performance is a Poor Metric for Verifying Convergence of Multi-agent Learning. *ArXiv abs/0904.2320* (2009). <https://api.semanticscholar.org/CorpusID:13515575>
- [2] Sherief Abdallah and Victor Lesser. 2008. A multiagent reinforcement learning algorithm with non-linear dynamics. *J. Artif. Int. Res.* 33, 1 (Dec. 2008), 521–549.
- [3] Dan Amir and Ofra Amir. 2018. HIGHLIGHTS: Summarizing Agent Behavior to People. In *Proceedings of the 17th International Conference on Autonomous Agents and MultiAgent Systems* (Stockholm, Sweden) (AAMAS '18). International Foundation for Autonomous Agents and Multiagent Systems, Richland, SC, 1168–1176.
- [4] Jupiter Bakakeu, Dominik Kisskalt, Joerg Franke, Shirin Baer, Hans-Henning Klos, and Joern Peschke. 2020. Multi-Agent Reinforcement Learning for the Energy Optimization of Cyber-Physical Production Systems. In *2020 IEEE Canadian Conference on Electrical and Computer Engineering (CCECE)*. 1–8. <https://doi.org/10.1109/CCECE47787.2020.9255795>
- [5] Kayla Boggess, Sarit Kraus, and Lu Feng. 2023. Explainable multi-agent reinforcement learning for temporal queries. In *Proceedings of the Thirty-Second International Joint Conference on Artificial Intelligence* (Macao, P.R.China) (IJCAI '23). Article 7, 9 pages. <https://doi.org/10.24963/ijcai.2023/7>
- [6] Alexandre Heuillet, Fabien Couthouis, and Natalia Díaz-Rodríguez. 2022. Collective eXplainable AI: Explaining Cooperative Strategies and Agent Contribution in Multiagent Reinforcement Learning With Shapley Values. *Comp. Intell. Mag.* 17, 1 (Feb. 2022), 59–71. <https://doi.org/10.1109/MCI.2021.3129959>
- [7] Kiarash Kazari, Ezzeldin Shereen, and György Dán. 2023. Decentralized Anomaly Detection in Cooperative Multi-Agent Reinforcement Learning. In *Proceedings of the Thirty-Second International Joint Conference on Artificial Intelligence (IJCAI-23)*. IJCAI.
- [8] Kiarash Kazari, Ezzeldin Shereen, and Gyorgy Dan. 2023. Decentralized Anomaly Detection in Cooperative Multi-Agent Reinforcement Learning. In *Proceedings of the Thirty-Second International Joint Conference on Artificial Intelligence, IJCAI-23*, Edith Elkind (Ed.). International Joint Conferences on Artificial Intelligence Organization, 162–170. <https://doi.org/10.24963/ijcai.2023/19> Main Track.
- [9] Wiem Khelifi, Siddarth Singh, Omayma Mahjoub, Ruan de Kock, Abidine Vall, Rihab Gorsane, and Arnú Pretorius. 2023. On Diagnostics for Understanding Agent Training Behaviour in Cooperative MARL. *arXiv:2312.08468 [cs.AI]* <https://arxiv.org/abs/2312.08468>
- [10] Ezgi Korkmaz and Jonah Brown-Cohen. 2023. Detecting adversarial directions in deep reinforcement learning to make robust decisions. In *Proceedings of the 40th International Conference on Machine Learning* (Honolulu, Hawaii, USA) (ICML '23). JMLR.org, Article 723, 10 pages.
- [11] Jakub Grudzien Kuba, Ruiqing Chen, Muning Wen, Ying Wen, Fanglei Sun, Jun Wang, and Yaodong Yang. 2022. Trust Region Policy Optimisation in Multi-Agent Reinforcement Learning. <https://arxiv.org/abs/2109.11251>
- [12] Tuan Le, Risal Shefin, Debashis Gupta, Thai Le, and Sarra Alqahtani. 2025. Verification-Guided Falsification for Safe RL via Explainable Abstraction and Risk-Aware Exploration. *arXiv:2506.03469 [cs.AI]* <https://arxiv.org/abs/2506.03469>
- [13] Jiahui Li, Kun Kuang, Baoxiang Wang, Furui Liu, Long Chen, Fei Wu, and Jun Xiao. 2021. Shapley counterfactual credits for multi-agent reinforcement learning. In *Proceedings of the 27th ACM SIGKDD Conference on Knowledge Discovery & Data Mining*. 934–942.
- [14] Simin Li, Jun Guo, Jingqiao Xiu, Yuwei Zheng, Pu Feng, Xin Yu, Aishan Liu, Yaodong Yang, Bo An, Wenjun Wu, and Xianglong Liu. 2023. Attacking Cooperative Multi-Agent Reinforcement Learning by Adversarial Minority Influence. *arXiv preprint arXiv:2302.03322* (2023).
- [15] Cameron Lischke, Tongtong Liu, Joe McCalmon, Md Asifur Rahman, Talal Halabi, and Sarra Alqahtani. 2022. Lstm-based anomalous behavior detection in multi-agent reinforcement learning. In *2022 IEEE International Conference on Cyber Security and Resilience (CSR)*. IEEE, 16–21.
- [16] Tongtong Liu, Joe McCalmon, Md Asifur Rahman, Cameron Lischke, Talal Halabi, and Sarra Alqahtani. 2022. Weaponizing actions in multi-agent reinforcement learning: Theoretical and empirical study on security and robustness. In *International Conference on Principles and Practice of Multi-Agent Systems*. Springer, 347–363.
- [17] Ryan Lowe, Yi Wu, Aviv Tamar, Jean Harb, Pieter Abbeel, and Igor Mordatch. 2017. Multi-Agent Actor-Critic for Mixed Cooperative-Competitive Environments. *Neural Information Processing Systems (NIPS)* (2017).
- [18] Joe McCalmon, Thai Le, Sarra Alqahtani, and Dongwon Lee. 2022. CAPS: Comprehensive Abstract Policy Summaries for Explaining Reinforcement Learning Agents. In *Proceedings of the 21st International Conference on Autonomous Agents and Multiagent Systems (AAMAS)*. IFAAMAS.
- [19] Dhouha Ben Noureddine, Atef Gharbi, and Samir Ben Ahmed. 2017. Multi-agent Deep Reinforcement Learning for Task Allocation in Dynamic Environment. In *International Conference on Software and Data Technologies*.
- [20] Martina Panfili, Alessandro Giuseppi, Andrea Fiaschetti, Homoud B. Al-Jibrean, Antonio Pietrabissa, and Franchisco Delli Priscoli. 2018. A Game-Theoretical Approach to Cyber-Security of Critical Infrastructures Based on Multi-Agent Reinforcement Learning. In *2018 26th Mediterranean Conference on Control and Automation (MED)*. 460–465. <https://doi.org/10.1109/MED.2018.8442695>
- [21] Haixia Peng and Xuemin Shen. 2021. Multi-Agent Reinforcement Learning Based Resource Management in MEC- and UAV-Assisted Vehicular Networks. *IEEE Journal on Selected Areas in Communications* 39, 1 (2021), 131–141. <https://doi.org/10.1109/JSAC.2020.3036962>
- [22] Vyacheslav Petrenko and Mikhail Gurchinskiy. 2021. Multi-agent deep reinforcement learning concept for mobile cyber-physical systems control. In *E3S Web of Conferences*, Vol. 270. EDP Sciences, 01036.
- [23] Risal Shahriar Shefin, Md Asifur Rahman, Thai Le, and Sarra Alqahtani. 2025. xSRL: Safety-Aware Explainable Reinforcement Learning - Safety as a Product of Explainability. In *Proceedings of the 24th International Conference on Autonomous Agents and Multiagent Systems* (Detroit, MI, USA) (AAMAS '25). International Foundation for Autonomous Agents and Multiagent Systems, Richland, SC, 1932–1940.
- [24] Jasper van der Waa, Jurriaan van Diggelen, Karel van den Bosch, and Mark Antonius Neerinx. 2018. Contrastive Explanations for Reinforcement Learning in terms of Expected Consequences. *ArXiv abs/1807.08706* (2018). <https://api.semanticscholar.org/CorpusID:49907182>
- [25] Minrui Xu, Jialiang Peng, B. B. Gupta, Jiawen Kang, Zehui Xiong, Zhenni Li, and Ahmed A. Abd El-Latif. 2022. Multiagent Federated Reinforcement Learning for Secure Incentive Mechanism in Intelligent Cyber-Physical Systems. *IEEE Internet of Things Journal* 9, 22 (2022), 22095–22108. <https://doi.org/10.1109/JIOT.2021.3081626>
- [26] Zhiwei Xu, Yunpeng Bai, Bin Zhang, Dapeng Li, and Guoliang Fan. 2023. HAVEN: Hierarchical Cooperative Multi-Agent Reinforcement Learning with Dual Coordination Mechanism. *Proceedings of the AAAI Conference on Artificial Intelligence* 37, 10 (Jun. 2023), 11735–11743. <https://doi.org/10.1609/aaai.v37i10.26386>
- [27] Xutong Zhao and Yaqi Xie. 2025. Multi-level Advantage Credit Assignment for Cooperative Multi-Agent Reinforcement Learning. *arXiv:2508.06836 [cs.AI]* <https://arxiv.org/abs/2508.06836>